How to cite: *Angew. Chem. Int. Ed.* **2024**, *63*, e202317549
doi.org/10.1002/anie.202317549

VIP Aqueous Li-ion Batteries Very Important Paper

Highly Efficient Spatially–Temporally Synchronized Construction of Robust Li_3PO_4-rich Solid–Electrolyte Interphases in Aqueous Li-ion Batteries

*Xiangzhen Zhu, Zejing Lin, Jingning Lai, Tianshi Lv, Ting Lin, Hongyi Pan, Jingnan Feng, Qiyu Wang, Shuai Han, Renjie Chen, Liquan Chen, and Liumin Suo**

Abstract: Solid electrolyte interphase (SEI) makes the electrochemical window of aqueous electrolytes beyond the thermodynamics limitation of water. However, achieving the energetic and robust SEI is more challenging in aqueous electrolytes because the low SEI formation efficiency (SFE) only contributed from anion-reduced products, and the low SEI formation quality (SFQ) negatively impacted by the hydrogen evolution, resulting in a high Li loss to compensate for SEI formation. Herein, we propose a highly efficient strategy to construct Spatially-Temporally Synchronized (STS) robust SEI by the involvement of synergistic chemical precipitation-electrochemical reduction. In this case, a robust Li_3PO_4-rich SEI enables intelligent inherent growth at the active site of the hydrogen by the chemical capture of the OH^- stemmed from the HER to trigger the ionization balance of dihydrogen phosphate ($H_2PO_4^-$) shift to insoluble solid Li_3PO_4. It is worth highlighting that the Li_3PO_4 formation does not extra-consume lithium derived from the cathode but makes good use of the product of HER (OH^-), prompting the SEI to achieve 100% SFE and pushing the HER potential into −1.8 V vs. Ag/AgCl. This energetic and robust SEI offers a new way to achieve anion/concentration-independent interfacial chemistry for the aqueous batteries.

[*] Dr. X. Zhu, Dr. Z. Lin, Dr. T. Lv, T. Lin, Dr. H. Pan, J. Feng, Dr. Q. Wang, S. Han, Prof. L. Chen, Prof. L. Suo
Beijing National Laboratory for Condensed Matter Physics, Institute of Physics, Chinese Academy of Sciences
Beijing 100190 (China)
E-mail: suoliumin@iphy.ac.cn

Dr. X. Zhu, Prof. L. Suo
Center of Materials Science and Optoelectronics Engineering, University of Chinese Academy of Sciences
Beijing 100049 (China)

Dr. X. Zhu, Prof. L. Suo
Yangtze River Delta Physics Research Center Co. Ltd.
Changzhou, Liyang 213300 (China)

Dr. J. Lai, Prof. R. Chen
Beijing Key Laboratory of Environmental Science and Engineering, School of Material Science & Engineering, Beijing Institute of Technology
Beijing 100081 (China)

Introduction

Aqueous lithium-ion batteries (ALIBs) built on mild aqueous electrolytes attract intense attention due to their intrinsic high safety, environmental friendliness, ease of manufacture, *etc.*[1–3] However, the limited electrochemical stability window (ESW) of water (1.23 V vs. SHE, at 25 °C, pH = 7, and 1 atm) and the severe hydrogen evolution reaction (HER) at the anode interface severely limit the development of high voltage (> 1.5 V) aqueous batteries, putting a cap on their energy densities.[4–5] Learning by the available commercial batteries, an effective strategy for HER suppression is to passivate the anode by forming a robust solid-electrolyte interphase (SEI), effectively preventing the continuous decomposition of water molecules by directly interacting with the anode surface, which can extend the electrochemical window of aqueous electrolytes beyond the thermodynamic constraint of water.[6–8] However, compared with non-aqueous organic electrolytes, it is much more challenging for the aqueous electrolyte to form a high-quality, robust SEI with high efficiency.[1,3] Detailedly, different from SEI in the non-aqueous electrolyte, the SEI contributor in ALIBs only originates from the reduction of salts or additives, and SEI chemical composition mainly consists of some inorganic compounds (LiF, Li_2CO_3, and Li_2O)[7,9–13] or organic/oligomeric species[12,14–16] derived from the reduction of the fluorinated bulky anions ($TFSI^-$, OTf^- and $BETI^-$, et al.),[7,11,17–19] dissolved gases (CO_2, and O_2),[10–11] or electrolyte components (organic co-solvents or additives),[12,14–16,20] whose formation is in a fierce battle with the HER of water solvent for electrons.[11,21] Moreover, forming these traditional SEI components in aqueous batteries still has many essential deficiencies. Firstly, the formation of fluorinated bulky anions-derived SEI is highly dependent on the high lithium salt concentration of the aqueous electrolyte (high Li:H_2O ratio, > 1:2.6), as the peculiar solvated structure of the high Li:H_2O ratio aqueous electrolytes can promote the electrochemical reduction of these fluorinated bulky anions.[7,9,11,17,21] Secondly, although the "common ionic effect" of dissolved lithium salts reduces the solubility of the inorganic salt-based SEI (LiF, Li_2CO_3, and Li_2O) in the concentrated aqueous electrolyte, its slightly dissolved behavior at the anode interface makes it difficult to effectively prevent contact between the electrolyte's water molecules and the anode surface.[10,22] As the electrolyte's water content increases, this detrimental effect

will be increasingly noticeable. Thirdly, the construction of Li-containing oligomer-based SEI significantly depends on the high organic co-solvent content and the low water content.[14,16] Nevertheless, the unrestricted reduction of the water content in the electrolyte by the addition of organic co-solvents deviates from the original goals of aqueous electrolytes, which included high safety, cheap cost, environmental friendliness, low viscosity, and high kinetic properties.

Based on those mentioned above, we can conclude that it is more challenging to generate an SEI in an aqueous electrolyte with good technical-economic performance because, on the one hand, the parasitic HER captures a higher proportion of electrons than the reduction reaction of SEI product, lowering the efficiency of batteries; on the other hand, the HER harms the growth of SEI and continuously destroy the gain because the intense gas evolution from the surface of anode makes the adhesion and nucleation of the reduced solid-state product more complex, resulting in much more Li consumption of the cathode electrode.[23–26] Therefore, one of the critical issues to achieving the practical application of aqueous batteries is how to build a high-quality SEI protective layer efficiently on the surface of the anode.

As we know, the HER will be accompanied by the generation of a large number of OH^- in the neutral electrolyte, resulting in an increase in the local concentration of OH^- at the anode surface.[5] Drawing from this understanding, we investigate the possibility that the OH^- could be chemically converted into insoluble SEI constituents, allowing us to construct Spatially-Temporally Synchronized (STS) robust SEI in aqueous batteries with remarkable efficiency. For this purpose, we attempt to introduce LiH_2PO_4(LHPO) into the anode, which can neutralize OH^- producing by water decomposition to chemically convert solid Li_3PO_4 phase at the electrode/electrolyte interface and achieve a high-efficiency STS Li_3PO_4-rich SEI layer formation. We demonstrated the practical application of the Li_3PO_4-rich SEI layer by constructing a 2.5 V aqueous full cell of $LiMn_2O_4$(LMO)//TiO_2@5 %LHPO in a 10 m LiTFSI electrolyte. Thanks to the low viscosity, the high ionic conductivity (33.4 mS cm^{-1}, 25 °C), and the low freezing point ((−12.5 °C) of the high water content electrolyte (10 m LiTFSI), the full cell exhibits excellent electrochemical performance, including excellent cyclic stability, super rate performance, and excellent low-temperature performance (−20 °C). Finally, we demonstrate that an ampere-hour (Ah)-level LMO//TiO_2@5 %LHPO pouch cell consistently delivers 50.7 Wh kg^{-1} of specific energy with high energy efficiency (≈90 %) at 1 C.

Results and Discussion

Figure 1a depicts the schematic illustration of our proposed mechanism for constructing STS Li_3PO_4-rich SEI layers. During the charging, the potential of the anode electrode gradually decreases to trigger the parasitic reactions, including the HER and the reduction of $TFSI^-$ anion to LiF.[7,13] As HER advances, OH^- accumulates on the anode electrode, and the dissolving $H_2PO_4^-$ effectively utilizes these by-products of hydrogen evolution to form the Li_3PO_4 SEI layer synchronously. As we know, weak polyprotic acid (such as H_2CO_3, $H_2C_2O_4$, and H_3PO_4, et al.) has an ionization equilibrium in an aqueous solution (the phosphoric acid was chosen to illustrate this ionization equilibrium), and the degree of ionization increases as the pH value rises due to the increase in the concentration of OH^- is going to deplete the H^+.[27–28] In the end, the final ionized products of the weak polyprotic acids will combine with Li cations to generate insoluble salts in the aqueous electrolyte (Figure S1). To further confirm the mechanism described in Figure S1, a simple chemical precipitation reaction experiment ($LiH_2PO_4 + 2LiOH \rightarrow Li_3PO_4\downarrow + 2H_2O$) is done to verify the final product. As shown in the inset digital photographs of Figure 1a, a white precipitate was generated once LiOH was added into the transparent aqueous solution of 1 m LiTFSI-LiH_2PO_4 (Figure S2), which is pure Li_3PO_4 powder verified by the X-ray diffraction (XRD) (Figure S3).

Unlike conventional SEI formation in aqueous electrolytes, our proposed STS Li_3PO_4-rich SEI formation has unique advantages. For one thing, our STS strategy has high efficiency with the low cost of Li. As mentioned above, the SEI formation in the aqueous electrolyte is a competing reaction where the parasitic HER consumes electrons without contributing to SEI formation. Assuming the electrons involved in all the parasitic reducing reactions at the anode are 100 % equal to the sum of the HER of x% and the SEI formation of 1-x% (Figure 1b). It means that the efficiency of SEI formation is highly susceptible to the HER. In our case, our STS strategy makes the HER product of OH^- chemically converted into the insoluble solid-state Li_3PO_4 deposition by the regulation of electrochemical decomposition and chemical deposition, thereby indirectly achieving 100 % utilization of electrons, reducing the irreversible Li loss from the cathode. For another thing, our STS strategy enables high-quality passivation to guarantee a uniform and denser SEI layer. The HER occurs at the site on the electrode accompanied by the byproduct of OH^- locally aggregates on the same reaction site where the exact right place of the passivation is the most needed. It gives the dissolving $H_2PO_4^-$ a perfect chance to space-time-synchronised capture the OH^- and in situ form Li_3PO_4-rich SEI in the right site. Besides, the selected recipe of Li_3PO_4 for our STS SEI formation not only has better ionic conductivity (10^{-5}–10^{-4} mS cm^{-1})[29] than LiF (10^{-6}–10^{-5} mS cm^{-1})[30] but also has high chemical stability with the lowest water solubility than LiF and Li_2CO_3 (Figure 1c, the detailed data is summarized in Table S1).

Figure 2a illustrates the ESW of 1 m LiTFSI and 1 m LiTFSI + 0.1 m LHPO aqueous electrolytes, as determined by linear sweep voltammetry (LSV) with a scanning rate of 10 mV s^{-1}. It shows that the 1 m LiTFSI + 0.1 m LHPO aqueous electrolyte has a higher hydrogen evolution potential ((−0.85 V vs. Ag/AgCl) than the 1 m LiTFSI aqueous electrolytes ((−1.52 V vs. Ag/AgCl) during the first scan process, because $H_2PO_4^-$ ionizes a portion of H^+ upon

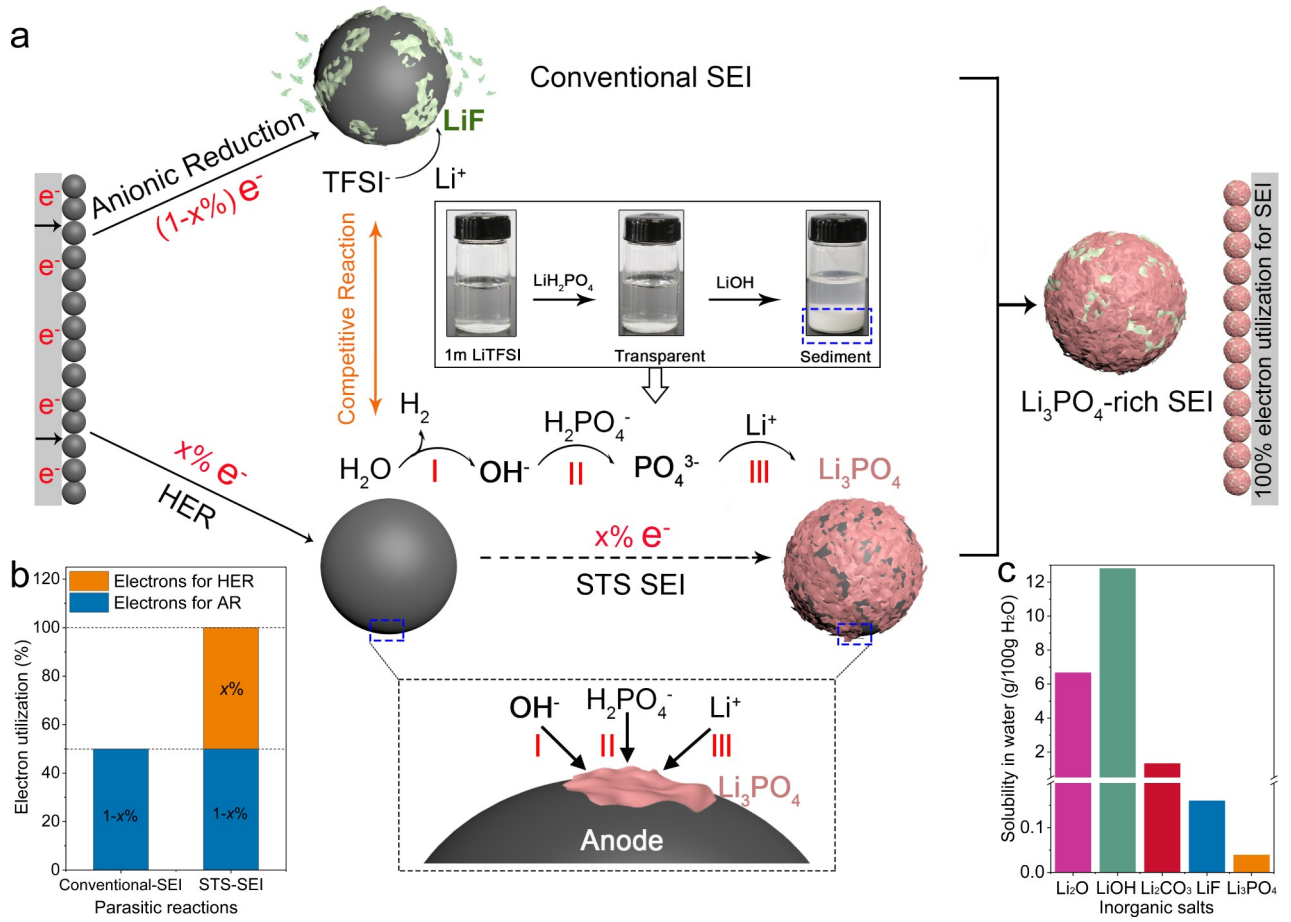

Figure 1. Proposing the strategy of STS Li_3PO_4-rich solid-electrolyte interphase (SEI) formation. (a) Illustrates the proposed STS constructing robust SEI mechanism. (*inset*: Chemical verification of the formation of Li_3PO_4.) (b) SEI formation efficiency (SFE) according to the electron utilization of the parasitic reaction electrons. (c) The solubility of inorganic Li salts in the water.

dissolution in the electrolyte, making the anode interface weakly acidic which is favorable for HER. After the first scanning process, the OH^- generated by the HER combines with H^+ to cause the ionization balance of $H_2PO_4^-$ to shift to PO_4^{3-}, eventually forming insoluble Li_3PO_4 coated on the surface of the Ti electrode. Therefore, during the second scan process, the 1 m LiTFSI + 0.1 m LiH_2PO_4 aqueous electrolyte demonstrates a lower hydrogen evolution potential (−1.90 V vs. Ag/AgCl). It is preliminary confirmation that manipulating the ion balance to form the passivation layer successfully prevents the HER from progressing, further expanding the ESW.

In comparison with the morphology of the cycled Ti electrode in the 1 m LiTFSI aqueous electrolyte detected by field emission scanning electron microscopy (FESEM, Figure 2b) and atomic force microscopy (AFM, Figure 2d), a thick passivating layer covered the surface of the Ti electrode in the 1 m LiTFSI + 0.1 m LHPO electrolyte (Figure 2c). Its huge morphology fluctuation (Figure 2e) indicates the existence of a compact SEI layer formation (The pristine Ti foil was exhibited in Figure S4). The element and chemical composition of the SEI layer on the Ti electrode was further evaluated by energy dispersive X-ray spectroscopy (EDX) mapping (Figure S5) and X-ray photoelectron spectroscopy (XPS), revealing homogeneous distributions of P and O elements on the surface of the SEI-Ti electrode and the chemical component was Li_3PO_4 (Figure 2f). Detailly, in the SEI-Ti electrode, the peak at 55.5 eV in the Li-1*s* spectra and the peaks at 134.3 eV and 133.4 eV assigned to two split components $2p_{1/2}$ and $2p_{3/2}$ in the P-2*p* spectra belongs to Li_3PO_4.[31] Besides, the XRD result of the SEI-Ti electrode (Figure S6) double-confirmed that the product on the Ti electrode surface is indeed Li_3PO_4. The results mentioned above demonstrate the feasibility of our STS SEI formation.

To further verify the effectiveness of our STS-SEI, the full cells of LMO//TiO_2@*x*%LHPO (*x* = 0, 5) with the various concentrated electrolytes (8 m, 10 m, and 21 m. The effectiveness of adding LHPO to the anode instead of the electrolyte is evaluated in the *Supporting Information* (Figure S7)) were tested (Figures 3a–3c and S8 (the detailed data was summarized in Tables S2 and S3)). The results depicted in Figure 3a demonstrate a notable enhancement in the initial Coulombic efficiency (ICE) when utilizing LMO//TiO_2@5 %LHPO, as compared to LMO//TiO_2, across various concentrations (8 m, 10 m, and 21 m). Specifically, the ICE values increased from 73.06 % to 88.27 % at 8 m, from

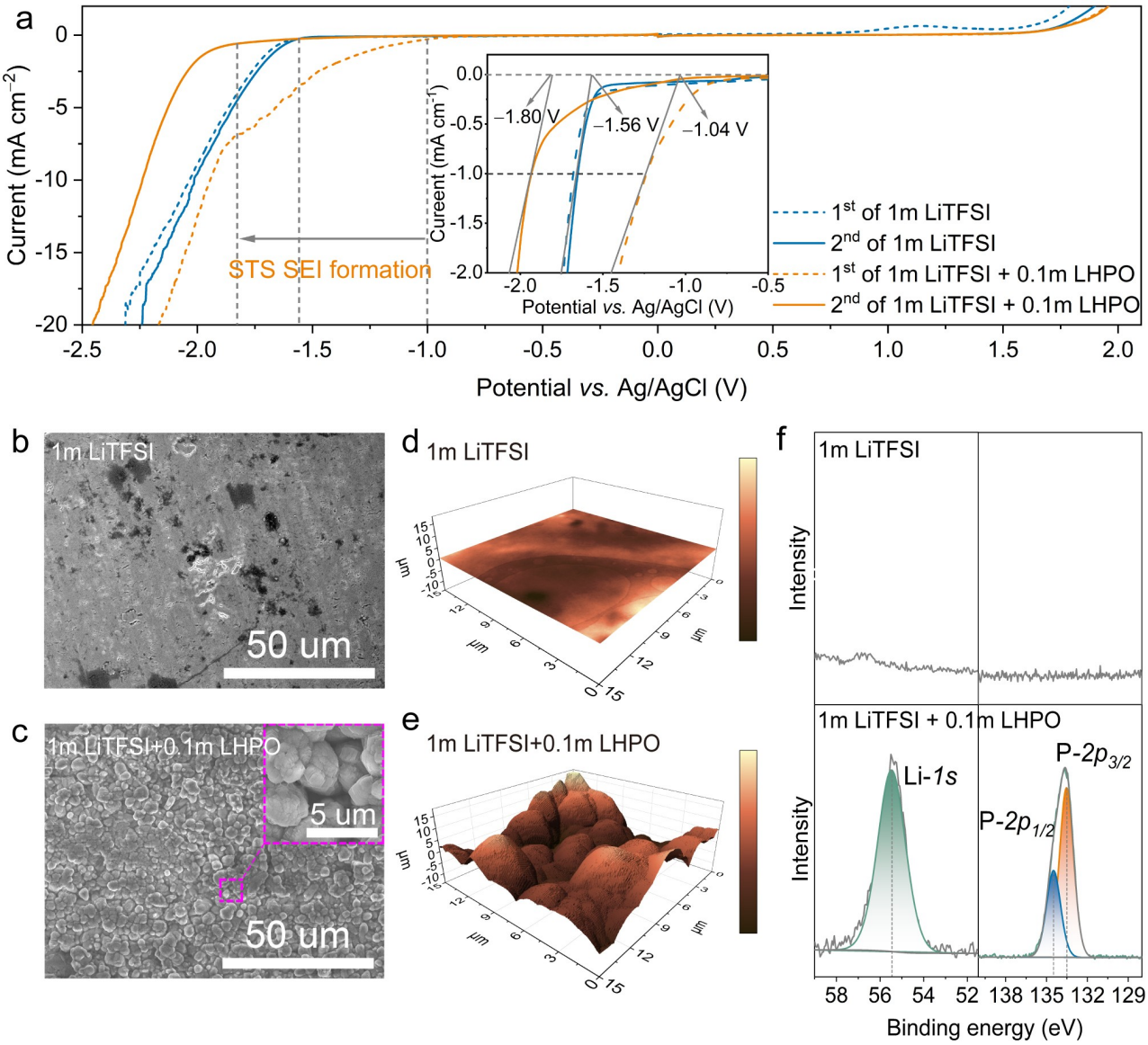

Figure 2. The Li_3PO_4-SEI formation in aqueous electrolytes (1 m LiTFSI and 1 m LiTFSI + 0.1 m LiH_2PO_4 in H_2O). (a) The electrochemical stability window of the 1 m LiTFSI and 1 m LiTFSI + 0.1 m LiH_2PO_4 aqueous electrolytes measured by LSV on the inactive collector Ti foil at 10 mV s^{-1}. The Ti foils after twice LSV scanning from 0 to −2.5 V are characterized, including field emission scanning electron microscopy (FESEM) images in the (b) 1 m LiTFSI + 0.1 m LiH_2PO_4 and (c) 1 m LiTFSI, atomic force microscopy (AFM) images in the (d) 1 m LiTFSI + 0.1 m LiH_2PO_4 and (e) 1 m LiTFSI, and (f) Li-1 *s* and P-2*p* X-ray photoelectron spectroscopy (XPS) spectra.

86.68 % to 91.83 % at 10 m, and from 90.03 % to 91.10 % at 21 m. These findings suggest that the incorporation of LHPO has a positive impact on the electrochemical performance, regardless of the electrolyte concentration. Figures 3b and 3c also show that the LMO//TiO_2@5 % LHPO improve significantly on average Coulombic efficiency (ACE) and capacity fading rate per cycle (CFR) compared to the LMO/TiO_2 in the whole concentration from 8 m (ACE: 81.84 %→95.08 %, CFR: 0.45 %→0.34 %), 10 m (ACE: 93.39 %→98.30 %, CFR: 0.39 %→0.04 %) to 21 m (ACE: 97.57 %→98.96 %, CFR: 0.03 %→0.01 %). It reveals that the increasing concentration positively impacts the CEs and cycle stability, but its profitability is gradually stable. Considering the high concentration would bring kinetic and low-temperature issues, our final concentration is balanced at 10 m to obtain comparable performance to conventional high-concentration WiS (21 m LiTFSI) electrolyte.[7] Meanwhile, the LMO//TiO_2@x%LHPO (x = 0, 2, 5, and 10) were optimized in aqueous batteries further in 10 m electrolyte (Figures 3d, 3e, and S9, the detailed data is summarized in Tables S2 and S3). It shows the amount of 2 *wt* % is insufficient to completely cover the TiO_2 anode, the SEI layer formed cannot entirely block the contact between water molecules in the electrolyte and the electrode, and an amount of 10 *wt* % is excessive inert material introduced into the electrode, inevitably reducing the aqueous battery's energy density. Thus, based on the above results, we fixed the 5 *wt* % as the best point for balancing

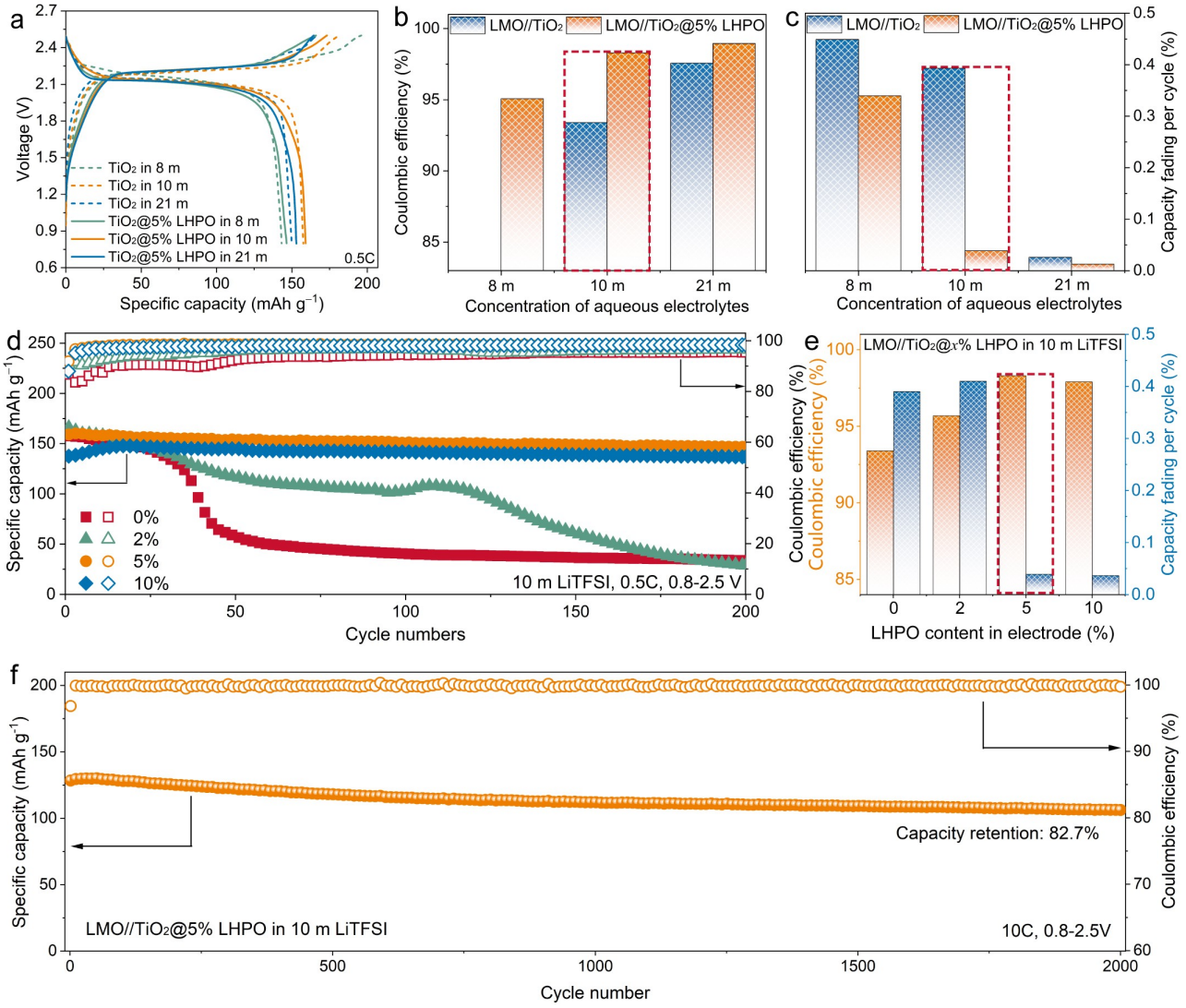

Figure 3. The electrochemical performance of the LMO//TiO_2@*x*%LHPO (*x* = 0, 2, 5, and 10) full cells (P/N mass ratio = 2:1). (a), (b) and (c) The charge–discharge curves with the various salt concentrations (8 m, 10 m, and 21 m LiTFSI) and their corresponding average Coulombic efficiency and capacity retention after 200 cycles. (d) and (e) The cycling performances and their corresponding average Coulombic efficiencies and capacity retentions after 200 cycles. (f) The long-term cycling stability of the LMO//TiO_2@5% LHPO full cell in 10 m LiTFSI aqueous electrolyte.

the electrochemical stability and energy density, exhibiting a high Coulombic efficiency (ACE: 98.30 %) and excellent cycle stability (CFR: 0.04 %). To further double-check our claims, Figure 3f shows the long-term cycle stability of LMO//TiO_2@5 %LHPO in 10 m LiTFSI electrolyte, whose capacity retention is above 82.7 % after 2000 cycles. It demonstrates the effectiveness of the STS-SEI in relatively low-concentrated electrolytes with such a low lithium-to-water ratio (Li:H_2O = 1:5.6 by molar ratio, Table S4), beneficial for solving the problems of high cost, high viscosity, and poor low-temperature performance caused by ultra-high salt concentration electrolytes (21 m LiTFSI, Li:H_2O = 1:2.6 by molar ratio).[7] When $H_2PO_4^-$ was replaced with HCO_3^-, the $LiMn_2O_4$//TiO_2@5 %$KHCO_3$ full cell showed a significant enhancement in Coulombic efficiency when compared to the $LiMn_2O_4$//TiO_2 full cell in 10 m LiTFSI electrolyte (Figure S10). Additionally, we assembled $LiMn_2O_4$//$Li_4Ti_5O_{12}$ and $LiMn_2O_4$//$Li_4Ti_5O_{12}$@5 %LHPO full cells; in the latter case, the STS-SEI strategy also demonstrated a more positive effect (Figure S11).

Considering that the kinetic protection offered by SEI is favorable to suppressing the decomposition of aqueous electrolyte, the in situ differential electrochemical mass spectrometry (DEMS) is applied to accurately detect H_2 and O_2 gas emissions at the different charge stages (Figure 4a). Compared with the cathode side, the aqueous electrolyte is susceptible to the irreversible reaction on the anode side because the HER is more severe and highly dependent on Charge of Stage (SOC) than oxygen evolution reaction (OER). For the control battery of LMO//TiO_2, the evolution rate of H_2 increased from 2.35 (baseline) to 6.24 nmol min^{-1} mg^{-1} at 2.5 V/SOC 100 %, and the total H_2 gas accumulation was 205.70 nmol mg^{-1} in the first cycle, whose tendency continuously enhances

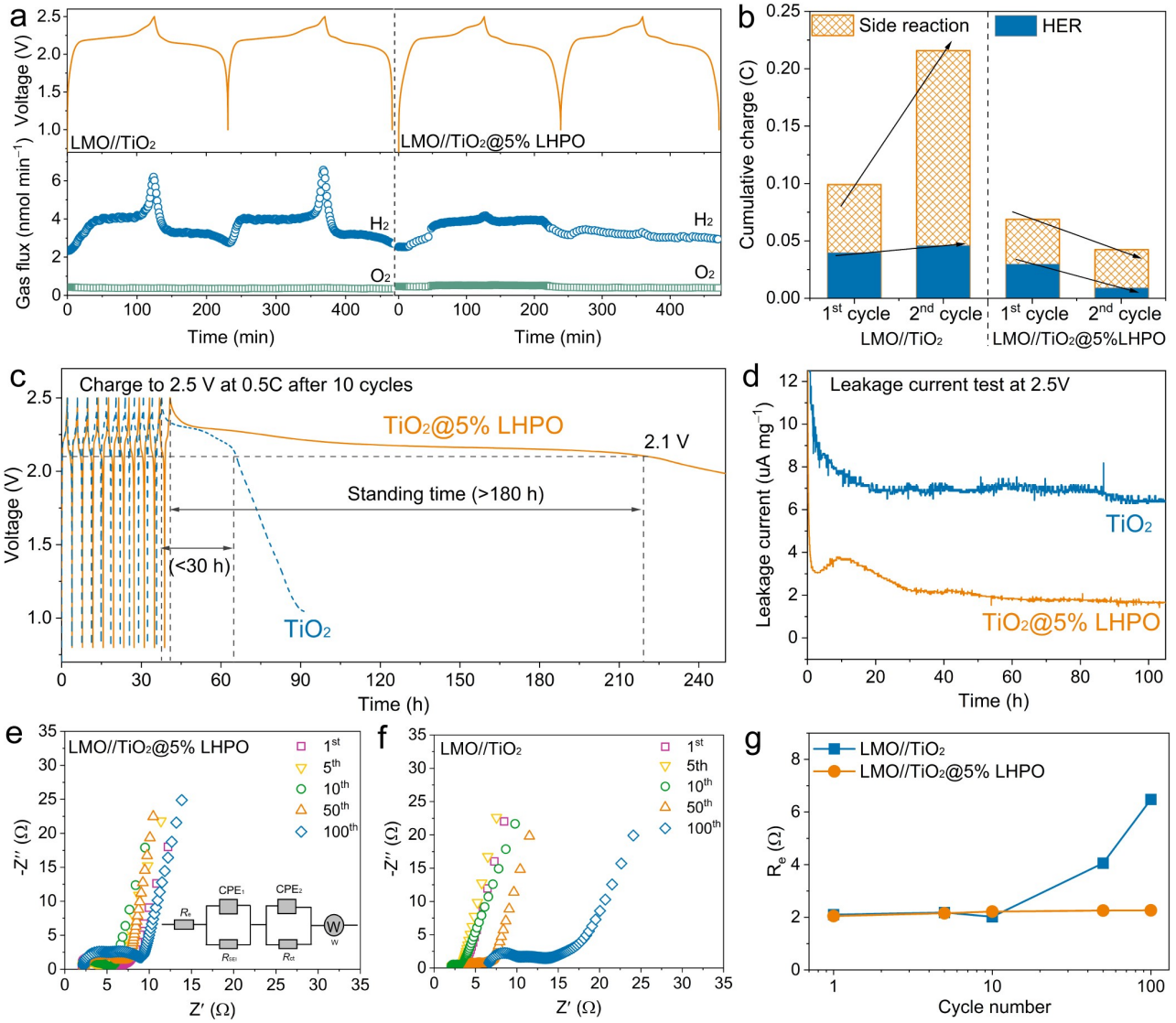

Figure 4. The SEI formation quality (SFQ) in full-cell batteries (LMO//TiO_2@5%LHPO, 10 m LiTFSI). (a) the H_2/O_2 gas evolution in the initial two cycles. (b) The cumulative charge of side reaction and HER was calculated based on the DEMS result of (a). (c) The self-discharge rate at 100% SOC. (d) The leakage current relaxation at a potentiostat 2.5 V. EIS of (e) LMO//TiO_2@5% LHPO (*inset*: Equivalent circuit for EIS modeling. R_e: bulk electrolyte resistance; R_{SEI}: surface film resistance; R_{ct}: charge transfer resistance; CPE_1 and CPE_2: constant-phase elements; W, Warburg impedance.) and (f) LMO//TiO_2 full cells with the cycle life. (g) The R_e values of EIS after 1, 5, 10, 50, and 100 cycles.

(6.59 nmol min^{-1} mg^{-1} at SOC 100%, and the total H_2 gas accumulation is 233.27 nmol mg^{-1}) in the following second cycle (Figure S12). Compared to LMO//TiO_2, the LMO//TiO_2@5%LHPO illustrates a much lower hydrogen evolution rate of 5.22 nmol min^{-1} mg^{-1} at 2.5 V/SOC 100% and the total hydrogen amount of 152.87 nmol mg^{-1} during the first cycle (Figure S13). More remarkably, the HER was significantly suppressed in the second cycle (H_2 evolution rate: 3.8 nmol min^{-1} mg^{-1} at 2.5 V/SOC 100%, and the total amount of H_2 gas: 45.19 nmol mg^{-1}, a reduction of nearly 50%), indicating that a robust STS-SEI layer with higher SFQ successfully formed on the surface of the TiO_2 electrode in the LMO//TiO_2@5%LHPO, which effectively suppressed HER. To discriminate how much the HER accounts for the overall faradic reaction in the batteries, the cumulative charge of HER and parasitic reaction are estimated and summarized in Figure 4b (For the detailed estimation, please see the Methods in the *Supporting Information*). It shows that, with the cycles, the cumulative charge of HER and side reaction of the LMO//TiO_2 increases. By contrast, both side reaction charges and the HER in the LMO//TiO_2@5%LHPO present a decline that further confirms the kinetic protection of our STS-SEI. According to the mechanism mentioned above, the OH^- produced by the HER can be buffered by the $H_2PO_4^-$ and lower the pH value for the TiO_2@5%LHPO electrode during cycles. As shown in Table S5, the pH of the TiO_2 electrode increased from 3.89 to 10.09 (strong alkaline) after ycles, whereas the pH of the TiO_2@5%LHPO electrode only increased from 2.30 to 8.20 (weakly alkaline),

implying the majority of the OH^- produced by the HER were consumed by the buffering effect of the $H_2PO_4^-$.

Since the SFQ has a decisive influence on the battery storage performances, several indicators are adopted to assess the storage performances, including the self-discharge, the leakage current (mA), and the electrolyte depletion time (cycle lifespan). The former two indicators are set up in harsh conditions (100 % SOC, 2.5 V) to evaluate the stabilization of electrolytes, and the latter indicator is to clarify the failure mechanism of aqueous electrolytes determined by SFQ. Figure 4c shows that the LMO//TiO_2@5 %LHPO has lower self-discharge with >180 h by recording the time the open circuit voltage dropped from the SOC 100 % 2.5 V to 2.1 V, and Figure 4d depicts an LMO//TiO_2@5 %LHPO with a significantly lower leakage current ($\approx$2.90 μA mg^{-1}) than the LMO//TiO_2 ($\approx$4.68 μA mg^{-1}) . Since the constant HER inevitably depletes the aqueous electrolyte, leading to increased impedance, the electrochemical impedance spectroscopy (EIS) is applied to observe the impedance accumulation arising from the TiO_2@5 %LHPO and TiO_2 electrodes (Figures 4e and 4f). Figure 4g summarizes the bulk electrolyte resistance (R_e) of LMO//TiO_2 and TiO_2@5 %LHPO originating from the fitting result of the equivalent circuit model. Even after long-term cycles, the minimal Re of TiO_2@5 %LHPO indicates that the electrolyte is kept in a relatively stable state due to the protective action of STS-SEI. In stark contrast, the R_e of LMO//TiO_2 increased rapidly after 10 cycles due to electrolyte depletion, whose viscosity increased progressively and whose ionic conductivity and wettability declined sharply as a result of the hydrogen evaluation results in continuous water consumption.

High-resolution transmission electron microscopy (HRTEM) shows no prominent SEI component on the surface of the cycled TiO_2 anode (Figure 5a) since the reaction of $TFSI^-$ reduction to generate LiF is inferior to the intense HER and high solubility of LiF in the relatively low concentrated electrolyte (10 m LiTFSI) with a high Li: H_2O molar ratio of 1:5.6. Fortunately, the high-efficiency STS constructing SEI methods used in this study efficiently resolve the issues above, and the resulting SEI layer on the TiO_2@5 %LHPO anode consisted of Li_3PO_4 and LiF species with a thickness of 5–10 nm (Figures 5b and 5c). According to the HRTEM image, Li_3PO_4 is primarily dispersed in the inner layer and occupies the majority of the total SEI layer, whereas LiF is attached to the outer layer of Li_3PO_4 or embedded in the gap of the Li_3PO_4-SEI layer and plays the role of repairing Li_3PO_4-SEI.

The chemical composition of the SEI on the TiO_2@5 % LHPO anode was further analyzed using XPS, and the results revealed that the main chemical components on the electrode surface were Li_3PO_4 and LiF. The peaks at 134.5 eV and 133.5 eV in the P-2*p* spectra of the TiO_2@5 % LHPO anode (Figure 5d) are assigned to two split components $2p_{1/2}$ and $2p_{3/2}$, corresponding to the phosphate group (PO_4^{3-}) of Li_3PO_4.[31] The F-1 *s* spectrum includes two peaks at 685.5 eV and 688.5 eV, corresponding to the LiF and -CF_2 groups in the PVDF binder.[7] According to XPS fitting, the proportions of Li_3PO_4 and LiF were 65.1 % and 34.9 %, respectively, indicating that a Li_3PO_4-rich SEI was successfully formed on the surface of the TiO_2@5 %LHPO anode (Figure 5f). Furthermore, time-of-flight secondary ion mass spectrometry (TOF-SIMS) was performed to investigate SEI′s chemical composition and element distribution on the cycled TiO_2@5 %LHPO anode. Their depth profile of the SEI under negative modes is depicted in Figure 5g. The variation in chemical speciation deep in the electrode was directly represented by the fluctuation in element count intensity vs. sputter time. PO_4^{3-} is observed in the spectrum as fragments containing P elements due to being sputtered by the Cs^+ beam. These fragments of negative species include PO_3^- (m/z = 79), PO_2^- (m/z = 63), PO^- (m/z = 47), P^- (m/z = 31) and F^- (m/z = 19). As expected, Li_3PO_4 (total P) content constantly held a higher level than LiF (F^-), which suggests that Li_3PO_4 accounts more than LiF for a larger proportion of SEI components. The presence of these species in the SEI layer is implied by the 2D TOF-SIMS element mapping shown in Figure 5h. These results confirm that Li_3PO_4 and LiF coexist in SEI components generated on the TiO_2@5 %LHPO anode.

Our stable STS-SEI formation in the low-concentrated electrolyte eliminates this obstacle, successfully allowing the 2.5 V full cells to operate in the 10 m LiTFSI electrolyte, providing considerable potential to improve the kinetic of aqueous batteries. As Figure S14 shows, the 10 m LiTFSI electrolyte exhibits an extraordinarily low viscosity (9.84 mPa s) and high ionic conductivity (33.4 mS cm^{-1}) at 25 °C, which is the highest value among all the wide electrochemical window electrolyte candidates (Table S4). Therefore, the LMO//TiO_2@5 %LHPO full cell with 10 m LiTFSI has excellent rate capability delivering the capacities of 160 mAh g^{-1} (0.5 C), 154 (1 C), 140 (2 C), 125 (5 C), 105 (10 C), 91 (20 C), and 68 (50 C) mAh g^{-1} respectively, and higher than the LMO/TiO_2 full cell with WiS-21 m LiTFSI has (Figures 6a and S15). Thanks to the protection of the robust STS-SEI layer, it enables the 10 m LiTFSI electrolyte with high-water content to be employed in the high voltage ALIBs (>2 V), which has low viscosity, low freezing point (−12.5 °C, Figure S16), and high ionic conductivities in the whole temperature range of −30 to 25 °C (Figure S14**)**. Even at −20 °C, this electrolyte maintains its low viscosity (168.64 mPa s) and high ionic conductivity (6.1 mS cm^{-1}), which is almost comparable to that of conventional WiS (21 m LiTFSI, 8.3 mS cm^{-1}) and WiBS (21 m LiTFSI + 7 m LiOTF, 6.1 mS cm^{-1}) electrolytes at 25 °C. Therefore, the LMO//TiO_2@5 %LHPO full cell demonstrates excellent low-temperature performance with high capacity retention and a small polarization at 0.5 C (Figure 6b and Figure S17). At −20 °C, our LMO//TiO_2@5 %LHPO full cell can still deliver a high specific capacity of 91.7 mAh g^{-1}, 56 % of its capacity at room temperature (25 °C) and superior cycle stability (89.2 % capacity retention after 400 cycles) with high average Coulomb efficiency of ≈99.9 % (Figure S18).

As illustrated in Figure 6c and Table S6, an Ah-level LMO//TiO_2@5 %LHPO pouch cell with a 1.0 Ah capacity (0.2 C) was successfully fabricated. Based on the entire weight of the pouch cell (43.21 g, Figure S19), the Ah-level

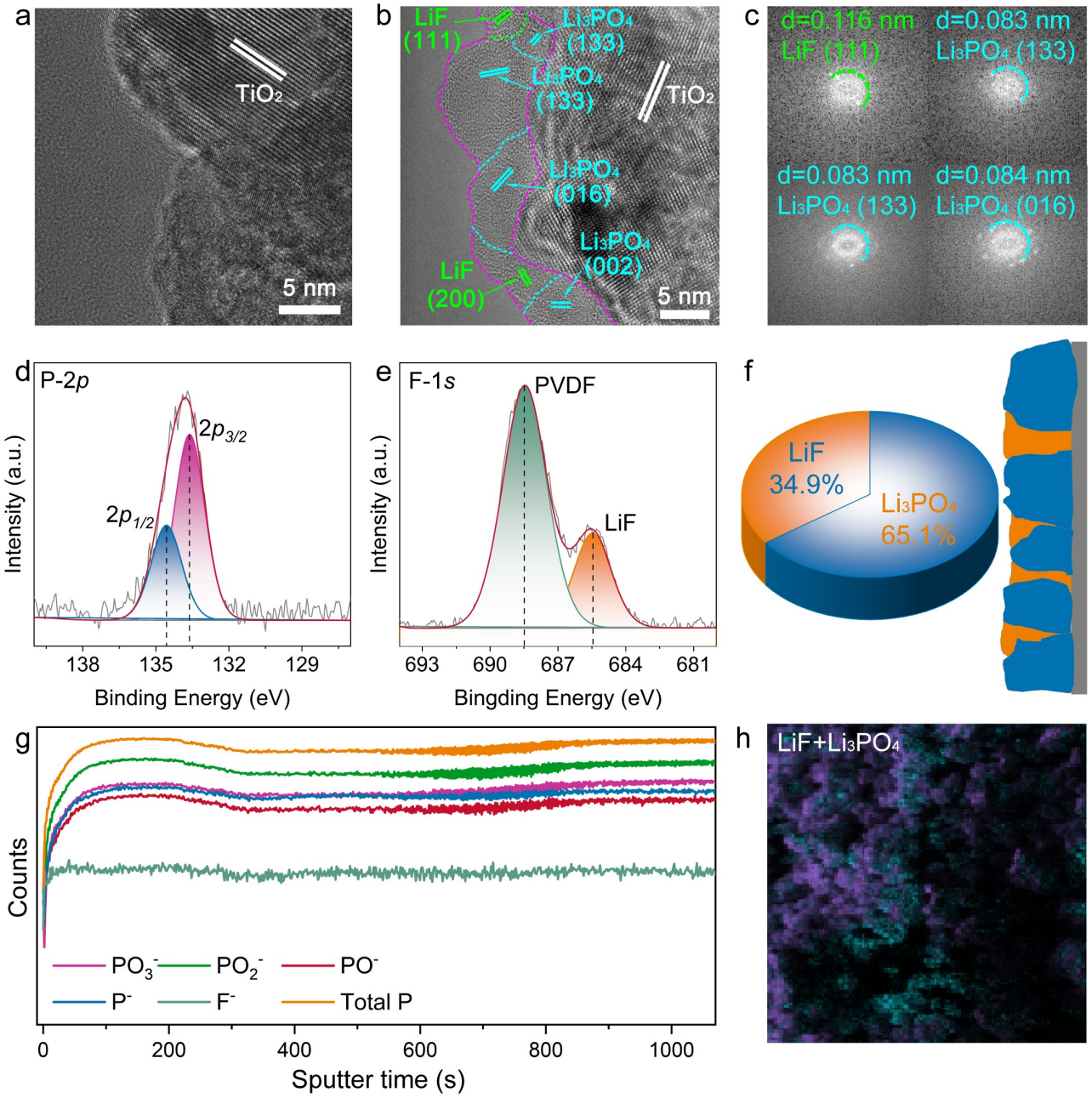

Figure 5. The Li_3PO_4-rich SEI formation on the cycled anode after 10 cycles at 0.5 C. HERTEM images of (a) TiO_2 and (b) TiO_2@5% LHPO electrodes. (c) FFT results of the cycled TiO_2@5% LHPO electrode. (d)–(f) The XPS spectra of the cycled TiO_2@5% LHPO electrode (g) and (h) the ToF-SIMS analysis of the cycled TiO_2@5% LHPO electrode.

pouch cell can deliver an energy density of 50.7 $Wh\,kg^{-1}$ (Figure 6d). In addition, the pouch cell exhibits excellent cycling stability with a capacity retention of 73.8% after 400 cycles and a high Coulombic efficiency of 99.8% at 1 C (Figure 6e), demonstrating that sustained cycle stability can be achieved even in large-scale energy storage applications. Despite the high area load of the cathode (17 $mg\,cm^{-1}$) and anode (10 $mg\,cm^{-1}$) active materials, the LMO//TiO_2@5% LHPO pouch cell shows small polarization and similar capacity release (140.7 $mAh\,g^{-1}$) to the mini cell due to the ultra-low viscosity of the 10 m LiTFSI electrolyte (Figure S20). In contrast, traditional high-voltage ALIBs usually show pronounced polarization due to the poor wetness and low ionic conductivity resulting from the ultra-high concentrated electrolytes, drastically affecting the capacity release and energy efficiency compared to the mini cells. The *inset* graph of Figure 6e depicts the charge–discharge energy efficiencies of the pouch cell at 1 C, as calculated by the energy absorbed and released. The pouch cell delivers a high average energy efficiency of ≈90% during the 200 cycles, meeting high-efficiency energy storage requirements. Due to the use of affordable TiO_2 and LMO as

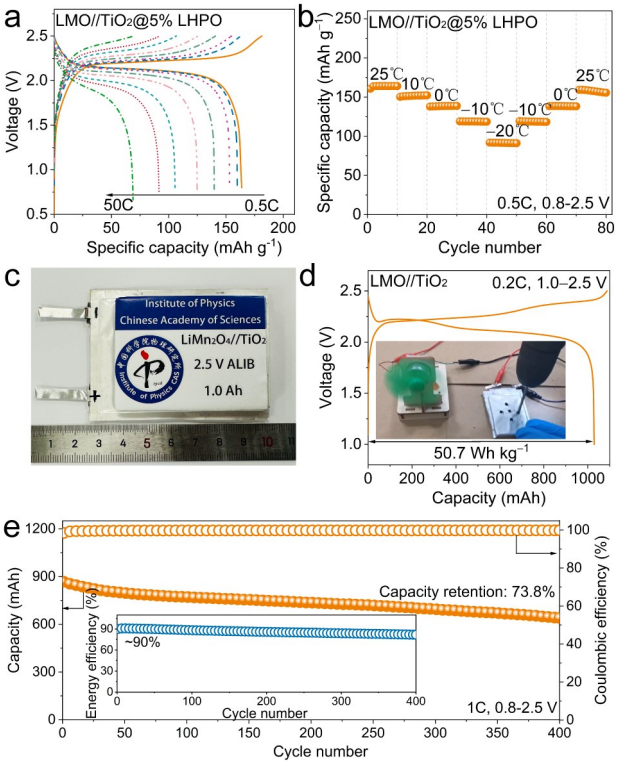

Figure 6. The electrochemical performance of the LMO//TiO_2@5% LHPO full cells in 10 m LiTFSI electrolyte. (a) Rate capability from 0.5 C to 50 C (b) low-temperature performance from 25 °C to −20 °C. (c) - (e) The 1 Ah level prototype full cell, (c) Photograph, (d) The first charge–discharge profile at 0.2 C (*inset*: drilling experiment video), and (e) The cycling stability at 1 C (*inset*: energy efficiency) of the LMO | 10 m LiTFSI | TiO_2@5%LHPO pouch cell.

electrode materials, the electrolyte concentration is reduced to less than half of the typical high-concentration salt electrolyte. Combined with these factors, the price of ALIB with a high voltage and energy density will undoubtedly be significantly reduced. Additionally, the Ah-level pouch cell exhibits superior safety performance. In the borehole test (*inset* of Figure 6d, Figure S21, and Video S1), the cell was able to keep a mini fan working continuously during the discharge process without any of the safety issues such as fire, explosion, or smoke that have afflicted non-aqueous lithium-ion batteries in the past.

Conclusions

In summary, we proposed highly efficient Spatially-Temporally Synchronized constructing robust solid-electrolyte interphase for aqueous batteries by regulating the ionization equilibrium of the multiple weak acid saline in an aqueous solution. We successfully established a Li_3PO_4-rich SEI interfacial protection layer on the surface of the anode in a high water-content electrolyte. With the excellent stability of Li_3PO_4 in water, even in an electrolyte with a high water content (10 m LiTFSI), the HER on the anode surface is successfully prevented, and for the first time, the smooth operation of a 2.1 V high-voltage ALIBs (LMO/TiO_2@5 % LHPO) in 10 m LiTFSI electrolyte is achieved. Together with a fast ionic conductivity of Li_3PO_4, LMO//10 m LiTFSI//TiO_2@5 %LHPO full cells present remarkable electrochemical reversibility, excellent rate capability, and praiseworthy long-term cycling stability. In addition, due to the low viscosity and freezing temperature of the 10 m LiTFSI electrolyte, the full battery shows outstanding low-temperature properties, with more than 56 % capacity maintained at −20 °C. An Ah-level pouch cell was fabricated and delivered a laudable electrochemical performance (50.7 Wh kg^{-1}) and outstanding safety, indicating the practical applications of this SEI fabrication strategy in high-voltage ALIBs.

Supporting Information

The Supporting Information is available free of charge.

Acknowledgements

All authors acknowledge the support of the National Key Research and Development Program of China (2022YFB2404500), the National Natural Science Foundation of China (U22B20124), and CAS Youth Interdisciplinary Team.

Conflict of Interest

The authors declare no conflict of interest.

Data Availability Statement

The data that support the findings of this study are available from the corresponding author upon reasonable request.

Keywords: Aqueous Batteries · Electrochemcial Window · Li_3PO_4 · Solid-Electrolyte Interphase

[1] W. Li, J. R. Dahn, D. S. Wainwright, *Science* **1994**, *264*, 1115–1118.
[2] J.-Y. Luo, W.-J. Cui, P. He, Y.-Y. Xia, *Nat. Chem.* **2010**, *2*, 760–765.
[3] A. von Wald Cresce, K. Xu, *Carbon Energy* **2021**, *3*, 721–751.
[4] D. Chao, W. Zhou, F. Xie, C. Ye, H. Li, M. Jaroniec, S.-Z. Qiao, *Sci. Adv.* **2020**, *6*, eaba4098.
[5] Y. Sui, X. Ji, *Chem. Rev.* **2021**, *121*, 6654–6695.
[6] E. Peled, S. Menkin, *J. Electrochem. Soc.* **2017**, *164*, A1703.
[7] L. Suo, O. Borodin, T. Gao, M. Olguin, J. Ho, X. Fan, C. Luo, C. Wang, K. Xu, *Science* **2015**, *350*, 938–943.
[8] J. Zhi, A. Z. Yazdi, G. Valappil, J. Haime, P. Chen, *Sci. Adv.* **2017**, *3*, e1701010.
[9] Y. Yamada, K. Usui, K. Sodeyama, S. Ko, Y. Tateyama, A. Yamada, *Nat. Energy* **2016**, *1*, 1–9.

[10] J. Yue, J. Zhang, Y. Tong, M. Chen, L. Liu, L. Jiang, T. Lv, Y.-s. Hu, H. Li, X. Huang, *Nat. Chem.* **2021**, *13*, 1061–1069.
[11] L. Suo, D. Oh, Y. Lin, Z. Zhuo, O. Borodin, T. Gao, F. Wang, A. Kushima, Z. Wang, H.-C. Kim, *J. Am. Chem. Soc.* **2017**, *139*, 18670–18680.
[12] Z. Hou, M. Dong, Y. Xiong, X. Zhang, Y. Zhu, Y. Qian, *Adv. Energy Mater.* **2020**, *10*, 1903665.
[13] N. Dubouis, P. Lemaire, B. Mirvaux, E. Salager, M. Deschamps, A. Grimaud, *Energy Environ. Sci.* **2018**, *11*, 3491–3499.
[14] Y. Shang, N. Chen, Y. Li, S. Chen, J. Lai, Y. Huang, W. Qu, F. Wu, R. Chen, *Adv. Mater.* **2020**, *32*, 2004017.
[15] J. Xu, X. Ji, J. Zhang, C. Yang, P. Wang, S. Liu, K. Ludwig, F. Chen, P. Kofinas, C. Wang, *Nat. Energy* **2022**, *7*, 186–193.
[16] R. Lin, C. Ke, J. Chen, S. Liu, J. Wang, *Joule* **2022**, *6*, 399–417.
[17] L. Suo, O. Borodin, W. Sun, X. Fan, C. Yang, F. Wang, T. Gao, Z. Ma, M. Schroeder, A. von Cresce, *Angew. Chem. Int. Ed.* **2016**, *128*, 7252–7257.
[18] X. Zhu, M. Mao, Z. Lin, J. Yue, M. Li, T. Lv, A. Zhou, Y.-S. Hu, H. Li, X. Huang, *ACS Materials Lett.* **2022**, *4*, 1574–1583.
[19] L. Chen, J. Zhang, Q. Li, J. Vatamanu, X. Ji, T. P. Pollard, C. Cui, S. Hou, J. Chen, C. Yang, *ACS Energy Lett.* **2020**, *5*, 968–974.
[20] F. Wang, O. Borodin, M. S. Ding, M. Gobet, J. Vatamanu, X. Fan, T. Gao, N. Eidson, Y. Liang, W. Sun, *Joule* **2018**, *2*, 927–937.
[21] S. Ko, Y. Yamada, A. Yamada, *ACS Appl. Mater. Interfaces* **2019**, *11*, 45554–45560.
[22] L. Droguet, G. M. Hobold, M. F. Lagadec, R. Guo, C. Lethien, M. Hallot, O. Fontaine, J.-M. Tarascon, B. M. Gallant, A. Grimaud, *ACS Energy Lett.* **2021**, *6*, 2575–2583.
[23] F. Wang, C.-F. Lin, X. Ji, G. W. Rubloff, C. Wang, *J. Mater. Chem. A* **2020**, *8*, 14921–14926.
[24] C. Yang, J. Chen, T. Qing, X. Fan, W. Sun, A. von Cresce, M. S. Ding, O. Borodin, J. Vatamanu, M. A. Schroeder, *Joule* **2017**, *1*, 122–132.
[25] J. Xie, Z. Liang, Y.-C. Lu, *Nat. Mater.* **2020**, *19*, 1006–1011.
[26] Y. Wang, T. Wang, D. Dong, J. Xie, Y. Guan, Y. Huang, J. Fan, Y.-C. Lu, *Matter* **2022**, *5*, 162–179.
[27] R. Moya-Hernández, J. C. Rueda-Jackson, J. Havel, M. T. Ramírez, G. A. Vázquez, A. Rojas-Hernández, *J. Chem. Educ.* **2002**, *79*, 389.
[28] R. A. Alberty, *J. Phys. Chem.* **1995**, *99*, 11028–11034.
[29] Y. A. Du, N. Holzwarth, *J. Electrochem. Soc.* **2007**, *154*, A999.
[30] X. Chen, S. Dou, W. Li, D. Liu, Y. Zhang, Y. Zhao, Y. Li, J. Zhao, X. Zhang, *Chem. Commun.* **2020**, *56*, 5018–5021.
[31] Y. Kobayashi, H. Miyashiro, K. Takei, H. Shigemura, M. Tabuchi, H. Kageyama, T. Iwahori, *J. Electrochem. Soc.* **2003**, *150*, A1577.

Manuscript received: November 17, 2023
Accepted manuscript online: December 11, 2023
Version of record online: December 21, 2023